
Article:
Nair, S., Wang, J. orcid.org/0000-0003-4870-3744, Chin, R. et al. (2 more authors) (2017) Analytical Prediction of 3D Magnet Eddy Current Losses in Surface Mounted PM Machines Accounting Slotting Effect. IEEE Transactions on Energy Conversion, 32 (2). pp. 414-423. ISSN 0885-8969

https://doi.org/10.1109/TEC.2016.2638477

Analytical Prediction of 3D Magnet Eddy Current Losses in Surface Mounted PM Machines Accounting Slotting Effect

Sreeju. S Nair, Student Member, IEEE, J. Wang, Senior Member, IEEE, R. Chin, L. Chen and Tianfu Sun Member, IEEE.

Abstract— This paper presents a novel analytical technique for predicting 3-dimensional (3D) magnet eddy current losses accounting the slotting effect of any pole–slot combinations for a surface mounted permanent magnet machine under any conditions of load. The slotting effect is incorporated from a subdomain model and the 3D boundary conditions are imposed with the current vector potential to represent the 3D eddy currents circulating in the magnets. The proposed model in polar coordinate system is demonstrated on a fractional slot rare-earth permanent magnet machine by analyzing its magnet losses as functions of axial and circumferential segmentations. The results have shown an excellent match with 3D numerical calculations. The analytical prediction has also been validated by experimental tests. The interaction of the armature reaction field with the slotting harmonics is analyzed and their effect on eddy current loss in rotor magnets is established. The proposed technique is employed to evaluate the effect of slotting on magnet loss with increase in field weakening angle.

Index Terms— Current vector potential, eddy currents, finite element, subdomain model, permanent magnet, 3D analytical.

I. INTRODUCTION

The rotor magnets of permanent magnet (PM) machines used in high speed and power density applications are exposed in increased rate of alternating magnetic field and incur eddy current loss. Eddy currents are more pronounced in magnets especially at higher speeds for such machines with modular or concentrated winding configurations [1, 2], as their stator magneto-motive force (mmf) contains a large number of space harmonics which rotate at different speeds along the rotor. Accurate prediction of magnet losses at the design stage, not only gives better efficiency evaluation, but also may prevent its excessive temperature rise and hence reduce the risk of partial demagnetization.

In order to evaluate the eddy current losses in permanent magnets, variety of methods have been reported in a large number in literatures. In general, evaluation of rotor eddy current losses requires simultaneous solutions for the governing equations of the magnetic and eddy current fields. The computationally efficient 2D numerical methods such as transient finite element analysis (FEA) to calculate the eddy current losses [3],[4] can yield good results but lacks any physical insight on the mechanism of eddy current loss. Hence a few 2D analytical methods are developed to predict the magnet eddy current loss with varying degree of accuracy [5-9]. These methods often neglect the slotting effect and approximate winding currents by an equivalent current sheet distributed over the stator bore radius.

Unless the slotting harmonics are considered in the loss evaluation, the no load magnetic loss and also its interaction with the armature filed harmonics at diverse load conditions cannot be quantified. As the eddy current density inside the magnets is dependent on the time derivative of the magnetic vector potential within it, a sufficiently accurate machine model becomes indispensable to estimate these time variations resulting from armature reaction and slotting effects. Magnet loss evaluation employing 2D relative permeance model [10, 11] gives an estimation of magnet losses at no load, but the results are deviating from the actual values when the loss due to armature reaction is accounted. While improved flux density assessment models are proposed in [12, 13] employing complex relative permeability, a more accurate subdomain models [14, 15] are preferred for loss estimation in permanent magnets [16, 17]. These methods except [6] and [11] are mainly resistance limited assuming the skin depth for the eddy currents is sufficiently larges than the wavelength of the alternating field under the normal operating conditions of the machine.

The accuracy of magnet loss evaluation is compromised in 2D evaluation methods if the axial length of magnets is comparable to their other dimensions since the eddy current flow in the magnets may become predominantly 3-dimensional (3D). This is further compounded by the introduction of axial segmentation [18] which makes the 3D –analysis indispensable. However, 3D FE models for prediction eddy current loss are usually complex to build, and their solutions require large memory and enormous computation time. To circumvent this problem, 3D analytical methods and reduced order numerical methods for calculation of eddy current loss have received significant interest in research communities[19-27]. These reduced order numerical methods may be computationally efficient, however complicated to implement. The 3D analytical methods are mostly established on simplifying assumptions which inevitably compromise their accuracy. Almost all the 3D analytical methods for

Sreeju S. Nair, J. Wang, L. Chen and Tianfu Sun are with the Department of Electronic and Electrical Engineering, The University of Sheffield, Sheffield, S1 3JD, UK (e-mail: ssnair1@sheffield.ac.uk, j.b.wang@sheffield.ac.uk, elq10lc@sheffield.ac.uk and elq12ts@sheffield.ac.uk)

R. Chin is with ABB Corporate Research, SE-721 78 Västerås, Sweden (e-mail: robert.chin@se.abb.com)

prediction eddy current losses in magnets in the literature fail to consider the slotting effect accurately and also ignores the field produced by the permanent magnets itself. Moreover, these methods also ignore the flux density field variation inside the magnet and neglect the instantaneous variation of loss among different magnet segments in computing the total eddy current loss.

This paper presents a novel analytical technique in polar coordinates for calculating the 3D magnet eddy current losses considering the slotting effect of any pole –slot combinations for a surface mounted permanent magnet machine under any conditions of load. Since the eddy current reaction effect becomes significant only at high operating frequencies [23], [28] the proposed method assumes resistance-limited eddy current in magnets and is sufficiently accurate for operating frequency up to a few kHz. The paper demonstrates analytical method of calculating joule losses in the magnet for an 8 pole 18 slot SPM motor, with due account of the effect of axial and circumferential segmentations at peak load operating conditions of the machine. The effect of slotting in reducing the magnet loss with increase in field weakening angle is comprehensively assessed using the proposed method.

II. Sub Domain Model and Calculation of Magnet Flux Density Variation

To account the slotting effect, the subdomain model, as shown in Fig. 1, [15] with simplified slots and uniform distribution of current in them is presented assuming infinitely permeable iron materials and replicates the flux density variations in the magnet quiet accurately. Since circumferential component of flux density is relatively small, its effect on eddy current loss is negligible [20]. The eddy current loss due to radial component of magnetic field is considered in this paper. The radial component of the flux density at a radius 'r' along the magnet [15], which contributes to the magnet loss can be represented as,

$$B_r = \begin{Bmatrix} -1/r \sum_k k\left(C_{1k} A_1 + C_{2k} M_{\alpha ck} - C_{3k} M_{rsk}\right)\sin\left(k\alpha\right) \\ +1/r \sum_k k\left(C_{1k} C_1 + C_{2k} M_{\alpha sk} + C_{3k} M_{rck}\right)\cos\left(k\alpha\right) \end{Bmatrix} \quad (1)$$

In the rotor reference $\alpha = \theta_r + \omega_r t$, and θ_r and ω_r are rotor position and angular speed, respectively. The values of C_{1k}, C_{2k} and C_{3k} are determined by the machine dimensions and are defined in [15]. The components directly related with magnetization viz. $M_{\alpha ck}, M_{rsk}, M_{\alpha sk}, M_{rck}$ can be expressed in rotor reference as,

$$\begin{aligned} &1/r\, C_{2k} k\left(-M_{\alpha ck}\sin\left(k\theta_r + k\omega_r t\right) + M_{\alpha sk}\cos\left(k\theta_r + k\omega_r t\right)\right) \\ &= 1/r\, C_{2k} k\left(M_{\alpha k}\cos\left(k\alpha_0 - k\theta_r\right)\right) \end{aligned} \quad (2)$$

$$\begin{aligned} &1/r\, C_{3k} k\left(M_{rsk}\sin\left(k\theta_r + k\omega_r t\right) + M_{rck}\cos\left(k\theta_r + k\omega_r t\right)\right) \\ &= 1/r\, C_{3k} k\left(M_{rk}\cos\left(k\alpha_0 - k\theta_r\right)\right) \end{aligned} \quad (3)$$

Substituting (2) and (3) into (1), and rearranging, the radial component of the flux density at a radius 'r' along the magnet which contributes to the magnet loss can be expressed in the rotor reference as

$$B_r = \sum_k \left[-C_k \cdot A_1 \sin\left(k\theta_r + k\omega_r t\right) + C_k \cdot C_1 \cos\left(k\theta_r + k\omega_r t\right)\right] \quad (4)$$

where

$$C_k = k/r \cdot C_{1k} \quad (5)$$

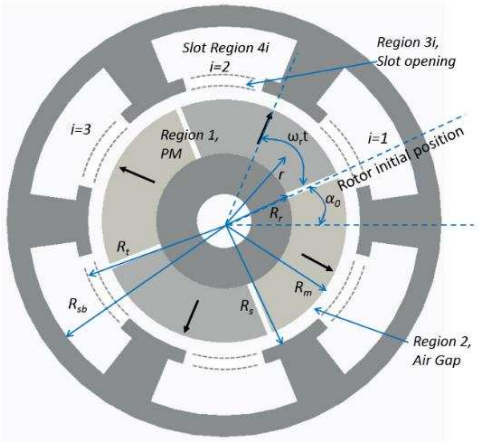

Fig.1 Subdomain model with illustration of key dimensional parameters.

The coefficients which accounts for the slotting effect, namely, A_1 and C_1 varies with rotor position and can be expressed as Fourier series:

$$A_1 = \sum_l a_{1l}\cos\left(lp\omega_r t + \psi_{al}\right) \quad (6)$$

$$C_1 = \sum_l c_{1l}\cos\left(lp\omega_r t + \psi_{cl}\right) \quad (7)$$

where l=1, 2, 3,… and p the number of pole pairs. a_{1l}, c_{1l} and ψ_{al}, ψ_{cl} are the magnitude and phase of the l^{th} harmonics of the two Fourier series.

Hence the radial flux density B_r can be rewritten as a combination of space and time harmonics as:

$$B_r\left(r,\theta,t\right) = \sum_k \sum_l C_k \begin{bmatrix} a_{br}\sin\left(k\theta_r + (k+lp)\omega_r t + \psi_{br}\right) \\ +a_{fr}\sin\left(k\theta_r + (k-lp)\omega_r t + \psi_{fr}\right) \end{bmatrix} \quad (8)$$

where

$$a_{br} = \left|-a_{1l}e^{j\psi_{al}} - c_{1l}e^{j(\psi_{cl}-\frac{\pi}{2})}\right| \Big/ 2 \quad (9)$$

$$a_{fr} = \left|-a_{1l}e^{-j\psi_{al}} + c_{1l}e^{-j(\psi_{cl}-\frac{\pi}{2})}\right| \Big/ 2 \quad (10)$$

$$\psi_{br} = \text{angle}\left(-a_{1l}e^{j\psi_{al}} - c_{1l}e^{j(\psi_{cl}-\frac{\pi}{2})}\right) \quad (11)$$

$$\psi_{fr} = \text{angle}\left(-a_{1l}e^{-j\psi_{al}} + c_{1l}e^{-j(\psi_{cl}-\frac{\pi}{2})}\right) \quad (12)$$

The definitions for other coefficients in (1)-(12) can be found in [15]. To express the B_r distribution in a 3D space, the flux density outside the axial length ($-l_M/2 \le z \le l_M/2$) of the machine is expanded in an odd Fourier series, as shown in Fig. 2. Thus, B_r can be expressed in (13) as Fourier series in z direction.

$$B_r\left(r,\theta,z,t\right) = \sum_\lambda B_r\left(r,\theta,t\right).4/\left(\pi\lambda\right).\sin\left(0.5\pi\lambda\right)\cos\left(\lambda\pi z/l_M\right) \quad (13)$$

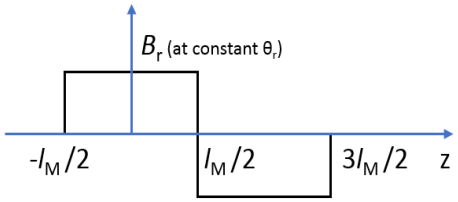

Fig.2 Periodic expansion of magnet flux density in axial (z) direction.

where λ =1, 3, 5,…and l_M is the magnet axial length. This expression ensures that the z-component of the eddy current density is zero at both axial ends of the magnet. The $\partial B_r/\partial t$ calculated from (13) forms the source for eddy current generation in the magnets and can be expressed as

$$\frac{\partial B_r}{\partial t}=\sum_{\lambda}\sum_{k}\sum_{l}\begin{Bmatrix}B_{rb}\cos(\lambda\pi z/l_M)\cos(k\theta_r+(k+lp)\omega_r t+\psi_{br})\\+B_{rf}\cos(\lambda\pi z/l_M)\cos(k\theta_r+(k-lp)\omega_r t+\psi_{fr})\end{Bmatrix} \quad (14)$$

where,

$$B_{rb}=a_{br}(k+lp)\omega_r C_k .4/(\pi\lambda).\sin(0.5\pi\lambda) \quad (15)$$

$$B_{rf}=a_{fr}(k-lp)\omega_r C_k .4/(\pi\lambda).\sin(0.5\pi\lambda) \quad (16)$$

III. Current Vector Potential and Formulation of Eddy Current Loss Calculation.

Since the divergence of the eddy current density $\vec{J}$ is zero, i.e. $\nabla\cdot\vec{J}=0$, this allows us to define a current vector potential $\vec{I}$ satisfying $\vec{J}=\nabla\times\vec{I}$ .The vector potential $\vec{I}$ must also satisfy $\nabla\cdot\vec{I}=0$ to ensure the net current in a magnet is zero. From Faraday's law:

$$\nabla\times\vec{J}/\sigma=\nabla\times(\nabla\times\vec{I})/\sigma=-\nabla^2\vec{I}/\sigma=-\partial B_r/\partial t \quad (17)$$

where σ is the conductivity of the magnets, and for the rare earth magnet under consideration it has a value of 5.556e5 S/m. (17) implies the $\vec{I}$ only has a radial component which satisfies:

$$1/r^2\,\partial^2 I_r/\partial\theta^2+\partial^2 I_r/\partial z^2=-\partial B_r/\partial t \quad (18)$$

It is evident that the accuracy of predicting $\vec{I}$ and, hence the eddy current loss calculation is dependent on the accuracy of the $\partial B_r/\partial t$ calculations. Since the eddy current flows in the tangential direction on all surfaces in a magnet, the current vector potential $\vec{I}(\theta_r,z,t)$ will be zero at all magnet surfaces. Hence the boundary conditions of (18) are given as:

$$\vec{I}(\theta_r=\theta_0)=\vec{I}(\theta_r=\beta_m+\theta_0)=0$$

$$\vec{I}(z=-l_M/2)=\vec{I}(z=l_M/2)=0$$

where θ_0 is the position of the starting edge of magnet under consideration. The geometric parameters of the magnet with segmentations is illustrated in Fig. 3. It is worth noting that the boundary condition of the eddy current density at the two cylindrical surfaces is automatically satisfied by the current vector potential formulation of (18).

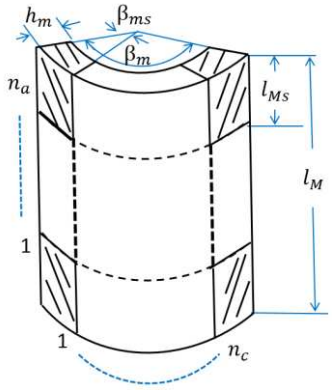

Fig. 3. Geometry of a magnet in cylindrical system.

The solution of (18) satisfying the boundary conditions are given by:

$$I_r(\theta,z,t)=-\sum_{\lambda}\sum_{k}\sum_{l}B_{rb}\frac{\cos(mz)}{(n^2+m^2)\cdot\sinh(mr\beta_m)}\cdot\begin{bmatrix}\sinh(mr(\theta_r-(\beta_m+\theta_0)))\cos(k\theta_0+(k+lp)\omega_r t+\psi_{br})\\-\sinh(mr(\theta_r-\theta_0))\cos(k(\beta_m+\theta_0)+(k+lp)\omega_r t+\psi_{br})\\+\sinh(mr\beta_m)\cos(k\theta_r+(k+lp)\omega_r t+\psi_{br})\end{bmatrix}$$
$$-\sum_{\lambda}\sum_{k}\sum_{l}B_{rf}\frac{\cos(mz)}{(n^2+m^2)\cdot\sinh(mr\beta_m)}\cdot\begin{bmatrix}\sinh(mr(\theta_r-(\beta_m+\theta_0)))\cos(k\theta_0+(k-lp)\omega_r t+\psi_{fr})\\-\sinh(mr(\theta_r-\theta_0))\cos(k(\beta_m+\theta_0)+(k-lp)\omega_r t+\psi_{fr})\\+\sinh(mr\beta_m)\cos(k\theta_r+(k-lp)\omega_r t+\psi_{fr})\end{bmatrix} \quad (19)$$

where $m=\lambda\pi/l_M$ and $n=k/r$. The axial component J_z and the circumferential component $J_{\theta r}$ of the eddy current at a radius 'r' can be derived as $J_z(t)=-1/r\cdot\partial I_r/\partial\theta_r$ and $J_{\theta r}(t)=\partial I_r/\partial z$ respectively. They are given in (20) and (21):

$$J_z(t)=\sum_{\lambda}\sum_{k}\sum_{l}B_{rb}\frac{\cos(mz)}{(n^2+m^2)\cdot\sinh(mr\beta_m)}\cdot\begin{bmatrix}m\cosh(mr(\theta_r-(\beta_m+\theta_0)))\cos(k\theta_0+(k+lp)\omega_r t+\psi_{br})\\-m\cosh(mr(\theta_r-\theta_0))\cos(k(\beta_m+\theta_0)+(k+lp)\omega_r t+\psi_{br})\\-k/r\sinh(mr\beta_m)\sin(k\theta_r+(k+lp)\omega_r t+\psi_{br})\end{bmatrix}$$
$$+\sum_{\lambda}\sum_{k}\sum_{l}B_{rf}\frac{\cos(mz)}{(n^2+m^2)\cdot\sinh(mr\beta_m)}\cdot\begin{bmatrix}m\cosh(mr(\theta_r-(\beta_m+\theta_0)))\cos(k\theta_0+(k-lp)\omega_r t+\psi_{fr})\\-m\cosh(mr(\theta_r-\theta_0))\cos(k(\beta_m+\theta_0)+(k-lp)\omega_r t+\psi_{fr})\\-k/r\sinh(mr\beta_m)\sin(k\theta_r+(k-lp)\omega_r t+\psi_{fr})\end{bmatrix} \quad (20)$$

$$J_{\theta r}(t)=\sum_{\lambda}\sum_{k}\sum_{l}B_{rb}\frac{m\sin(mz)}{(n^2+m^2)\cdot\sinh(mr\beta_m)}$$
$$\cdot\begin{bmatrix}\sinh\left(mr(\theta_r-(\beta_m+\theta_0))\right)\cos\left(k\theta_0+(k+lp)\omega_r t+\psi_{br}\right)\\-\sinh\left(mr(\theta_r-\theta_0)\right)\cos\left(k(\beta_m+\theta_0)+(k+lp)\omega_r t+\psi_{br}\right)\\+\sinh(mr\beta_m)\cos\left(k\theta_r+(k+lp)\omega_r t+\psi_{br}\right)\end{bmatrix}$$
$$+\sum_{\lambda}\sum_{k}\sum_{l}B_{rf}\frac{m\sin(mz)}{(n^2+m^2)\cdot\sinh(mr\beta_m)}$$
$$\cdot\begin{bmatrix}\sinh\left(mr(\theta_r-(\beta_m+\theta_0))\right)\cos\left(k\theta_0+(k-lp)\omega_r t+\psi_{fr}\right)\\-\sinh\left(mr(\theta_r-\theta_0)\right)\cos\left(k(\beta_m+\theta_0)+(k-lp)\omega_r t+\psi_{fr}\right)\\+\sinh(mr\beta_m)\cos\left(k\theta_r+(k-lp)\omega_r t+\psi_{fr}\right)\end{bmatrix} \quad (21)$$

The eddy current loss in a magnet can be derived as the sum of each harmonic loss considering the flux density variations at different radial distances throughout the entire radial thickness (h_m) of the magnet. The total magnet loss considering segmentation in the machine at any time instant can be approximated by averaging a magnet segment loss evaluated at these radial distances and multiplying with the total number of magnet segments as:

$$Pe(t)=\frac{1}{N_r}\sum_{Rr}^{Rm}\sum_{\lambda}\sum_{k}\sum_{l}\frac{h_M n_c n_a}{\sigma}\int_{\theta_0}^{\beta_{ms}+\theta_0}\int_{-l_{Ms}/2}^{l_{Ms}/2}\left(Js_{\theta_r}^2+Js_z^2\right)\cdot rd\theta_r\cdot dz. \quad (22)$$

where N_r is the number of radial position considered in the computation and n_a and n_c are number of axial and circumferential segments considered respectively. Also Js_{θ_r} and Js_z are the axial and circumferential component of current density evaluated for the magnet segment. However, a better approximation can be obtained by computing the sum of loss in each magnet segment separately and adding them together to find the total magnet loss at different time instants. Because time varying eddy current densities repeats 6 times in a fundamental electric period, it is necessary to calculate the eddy current loss at least for one sixth of the electrical period to obtain the average value.

IV. Validation by Finite Element Analysis

The developed 3D eddy current loss prediction technique is applied to an 18-slot 8-pole surface mounted PM machine with winding configuration shown in Fig.4. The machine employs winding design features [29] to reduce space harmonics and hence reduced rotor eddy current loss, while retaining the merits of fractional slot per pole machine topology. The key geometrical, physical parameters and specifications are listed in Table 1 where the key design data for a 12-slot, 14-pole SPM machine used in experimental validation are also given. To validate the developed model, the magnetic field distribution and eddy current loss are also predicted by 2D/3D time–stepped transient FE analysis with the models shown in Fig. 5.

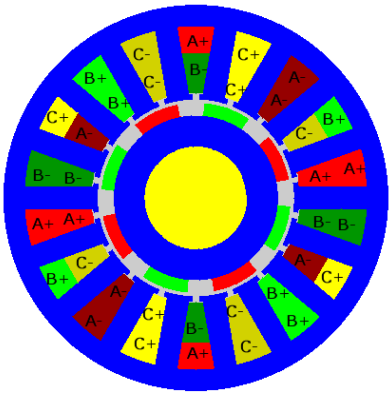

Fig. 4. 18-slot 8-pole machine with fractional-slot per pole winding configuration.

TABLE I
Specifications and key dimensions of SPM machines

Parameter	Unit	18 slot 8 pole	12slot, 14 pole
Continuous power	kW	5	5
Peak power	kW	10	7
Base speed	rpm	1350	1350
Maximum speed	rpm	4500	4500
Stator outer radius	mm	75.0	75.0
Motor stack length	mm	118	122
Air gap length	mm	0.955	0.955
Rotor radius	mm	37.5	41.25
Magnet length	mm	5.0	5.0
Slot opening	mm	2.03	3.75
Slot opening depth	mm	2.375	3.67
Slot depth	mm	26.79	26.04
Shaft radius	mm	20.0	25
Magnet resistivity	Ω.m	1.8×10^{-6}	1.6×10^{-6}

The eddy current and the associated loss are evaluated when the machine is operated at its peak load conditions with peak phase current of 80A at 4500rpm. Before the eddy loss in the magnets is evaluated by the developed analytical technique, it is insightful to have confidence on the analytically predicted source of eddy current generation $\partial B_r/\partial t$. The analytically and 2D FE predicted $\partial B_r/\partial t$ variations with θ_r at r= 37.5mm, 35.0mm and 32.5mm, at $\omega_r t = 1.25^0$ of magnet '1' is compared in Fig.6, Fig.7 and Fig.8, respectively. As can be seen, the $\partial B_r/\partial t$ predicted by the subdomain model considering slotting effect has shown good accuracy with the 2D transient FE analysis at the peak load. The slight difference is visible at the magnet inner surface due to core saturation which is neglected in the analytical model and also due to the simplified slot shaping [15] used in the subdomain model.

3D transient FE analysis is also carried out in Flux 3D using the model shown in Fig.3 to predict eddy current density distribution and eddy current loss in magnets. Since the machine employs fractional slot per pole topology,

circumferential symmetry exits only over 180 mechanical degrees. Thus, a quarter of the machine has to be modelled in 3D FEAs. Tangential magnetic field boundary condition is imposed on the end surfaces perpendicular to the axial direction. In addition, perfect insulation boundaries are applied to the end surfaces of the magnets.

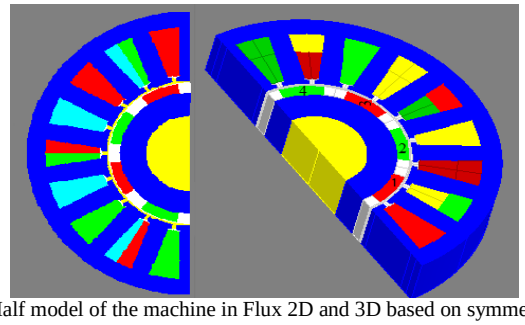

Fig. 5. Half model of the machine in Flux 2D and 3D based on symmetry.

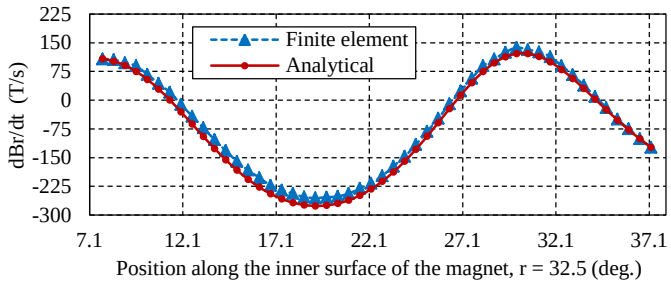

Fig. 6. $\partial B_r/\partial t$ Comparison of F.E and slotting effect model at outer surface.

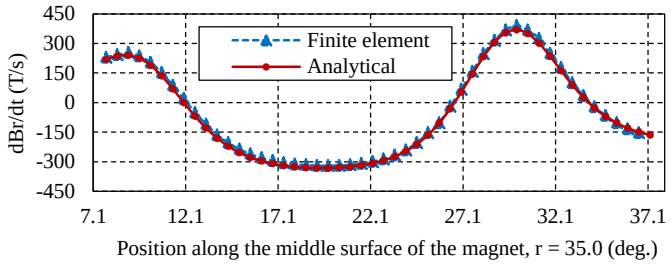

Fig. 7. $\partial B_r/\partial t$ Comparison of F.E and slotting effect model at middle surface.

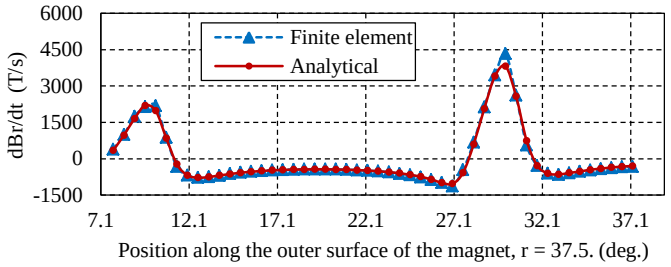

Fig. 8. $\partial B_r/\partial t$ Comparison of F.E and slotting effect model at inner surface.

Fig.9 and Fig.10 compares the analytically and 3D FE predicted eddy current density distribution at the outer cylindrical surface of the magnet '1' indicated in the Fig.3 which is located at an angle of 24^0 at time =55.5μs when the machine is having two axial magnet segmentation and rotating at the speed of 4500 rpm. Similar comparison is given in Fig.11 and Fig.12 for analytically and 3D FE predicted eddy current density distributions at the inner surface of the magnet '1'. It can be observed that the current density distribution from the analytical computation is matching with 3D FE with a good accuracy, except for few meagre mismatches especially along the inner surface of the magnet, as a result of the $\partial B_r/\partial t$ discrepancy shown in Fig.8.

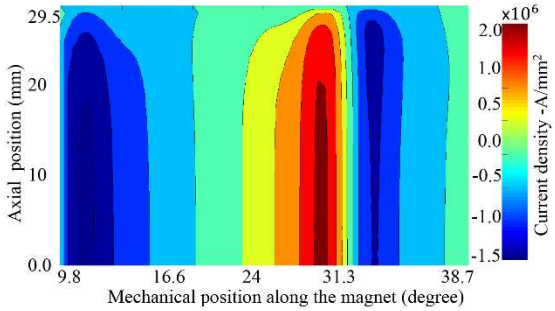

Fig. 9. Current density from analytical 3D, on the magnet outer surface.

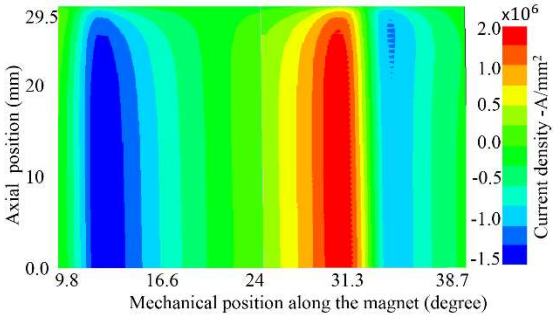

Fig. 10. Current density from F.E-3D on the magnet outer surface.

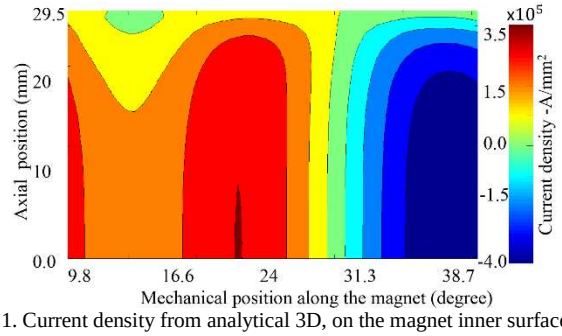

Fig. 11. Current density from analytical 3D, on the magnet inner surface.

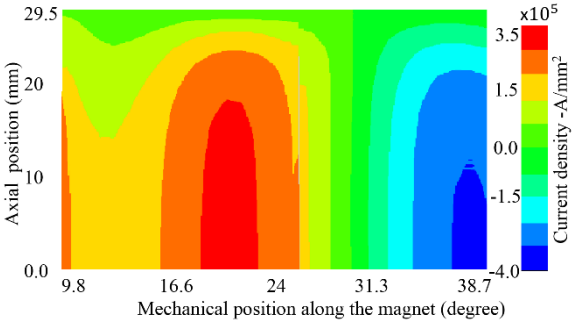

Fig. 12. Current density from F.E-3D on the magnet inner surface.

The analysis is repeated with different number of circumferential and axial segments at the same operating conditions of the machine. The results from 3D analytical, 3D FE and 2D FE for different axial segmentations with one and two circumferential segments at peak load conditions are compared in Fig.13 and Fig.14. The variation of magnet loss from 3D analytical, 3D FE and 2D FE for different

circumferential segmentations with one axial segment at the peak load condition are compared in Fig.15.

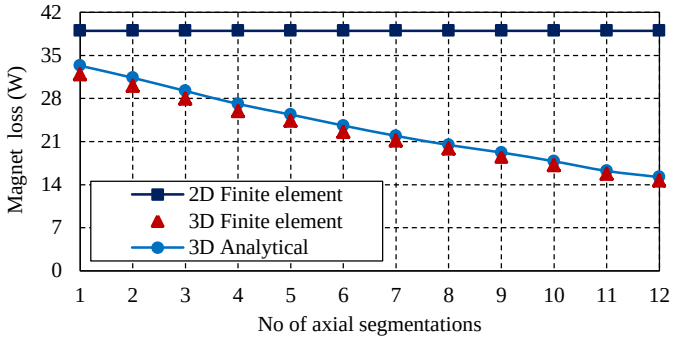

Fig. 13. Magnet losses comparison- peak load (Circumferential segments: 1).

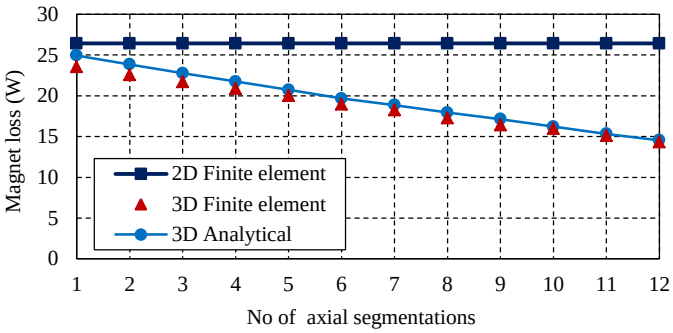

Fig. 14. Magnet losses comparison- peak load (Circumferential segments: 2).

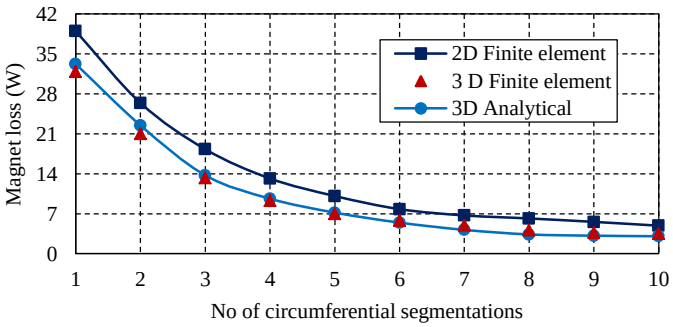

Fig. 15. Magnet losses comparison- peak load (Axial segments: 1).

It is evident that the analytical predictions agree very well with the 3D FE results. The minor deviation of the analytical predictions from the 3D FE results can be attributed to neglecting the tangential component of flux density in the loss prediction and the error $\partial B_r/\partial t$ in prediction. In contrast, significant errors occur in 2D FE eddy current loss predictions.

For the 18-slot, 8-pole machine under consideration the radial positions N_r is chosen as 50 while evaluating the 3D magnet loss from (22). The percentage difference when the number of radial position is increased to 60 is only 0.247% with respect to the results obtained when $N_r = 50$. However the computation time for the magnet loss prediction per case is increased by 7 minutes when N_r is increased from 50 to 60. This shows the usage of more radial samples may results only in marginal improvement of accuracy at the expense of more time consumed. The computation time for the subdomain model to extract the flux density information at each operating condition is close to 22.45 minutes. While the computation time for the analytical model to predict the magnet loss at each operating condition per case is about 20.5 minutes ($N_r = 50$) on a 64 GB RAM desktop computer (3.3 GHz, I7 processor with 6 cores) in Matlab environment. However, it takes more than 60 hours for 3D FE with no axial segmentations ($n_a = 1$) and almost 10 hours with 12 axial segmentations ($n_a = 12$) on the same desktop computer using CEDRAT- FLUX 3D.

V. Experimental Validation

Experimental validation of rotor eddy current loss prediction is quite challenging because the amount of eddy current loss in a well-designed machine is relatively small, and it is very difficult to separate the eddy current loss from iron loss and mechanical loss by direct measurements.

The indirect magnet loss measurement was reported in [4] for PM machines based on the rate of temperature rise measured by temperature sensors through slip rings, but the technique has poor accuracy as a result of contact resistance variations associated with slip rings and brushes. Further, the method can only estimate the loss based on the thermal property and geometry of the magnets, and its accuracy is often affected by no-uniform temperature distribution in the magnets as well as possible heat exchanges with other regions[30].

To overcome these problems, we have devised experimental validation of the developed eddy current loss prediction technique by direct loss measurements under locked rotor conditions. Experiments are performed on a 12-slot, 14-pole surface mounted PM (SPM) machine designed for electric vehicle applications [31]. Two SPM rotors are constructed, one with un-magnetized magnets and the other without magnets. The prototype rotor with assembled magnets contains three axial segments and one circumferential segment per pole. The key geometrical, physical parameters and specifications of the machine are listed in Table I. The prototyped rotors, fully assembled machine with rotor locked and the whole experimental set is illustrated in Fig.16.

Initially the testing was carried at the locked rotor condition with the rotor in which no magnets are assembled. The machine windings were supplied with 45A (peak) phase currents at 400Hz.The experiment was repeated using the rotor assembled with permanent magnets for the same phase current and the measurements were taken at the same winding temperatures as measured in the previous case without magnets. Therefore, the flux distribution in the machine was kept virtually the same for both the experiments as the magnets were not magnetized while performing the second test. For both the tests power input to the machine was measured from the power analyzer and phase current waveforms were captured using the oscilloscope. The same experiments were also repeated when the machine windings were supplied with 50A peak phase currents at 400Hz. The magnets loss at the given current conditions is evaluated from the difference in power input to the machine measured from the corresponding experiments with and without rotor magnets. In addition, the correction to the measured loss is

applied to account for the difference in copper loss due to a minor change in the fundamental phase currents measured from the experiments with and without magnets. The phase currents measured from the experiments at 45A and 50A are shown in Fig.17.

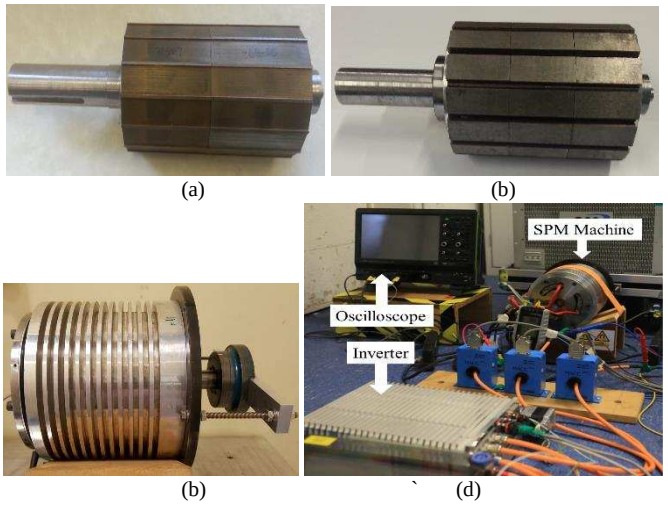

Fig 16. Prototype rotors and experimental setup. (a) without magnet. (b) with magnet. (c) machine assembly with locked rotor. (d) Experimental setup.

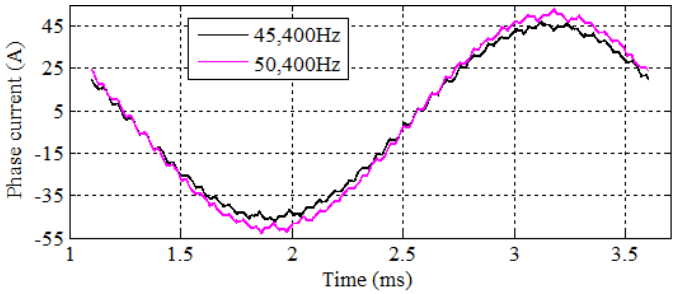

Fig.17.Phase currents measured from the experiments at 400Hz (45 and 50A).

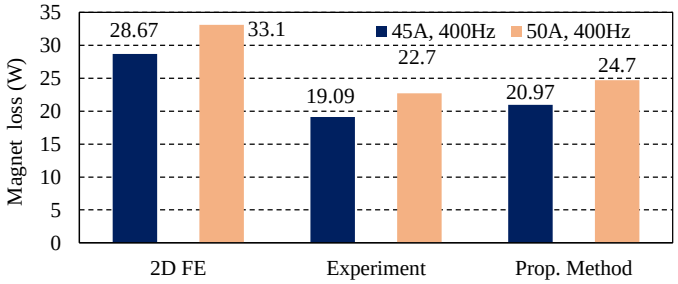

Fig.18. Comparison of magnet loss from the experiments, proposed 3D method and 2D FE at both the phase currents at 400Hz.

These phase currents measured from the experiments are employed as the input to the subdomain model for generating the flux density information within the magnet. 3D magnet loss is evaluated at the stand still conditions of the rotor for both the currents employing the proposed method. The comparison of the magnet losses obtained from the experiment, the proposed 3D method and 2D FE is shown in Fig.18. It is observed that the experimental results agree closely with the results obtained from the proposed 3D method, while significant error is evident with results obtained from 2D FE. The mismatch in the results obtained from the experiment and the analytical 3D method can be attributed to the eddy current reactions associated with higher order switching harmonics, which is neglected in the proposed method. The difference in measured and predicted losses may also be attributed to the end winding effect which is neglected in the proposed method and to the minor variations in the iron loss between the two tests.

VI. Effect of Slotting in Reducing Magnet Loss at Field Weakening

It is well known that the eddy current loss in the rotor magnets are contributed by both armature reaction field and slotting effect. Under some load conditions such as field weakening, slotting effect reduces the total eddy current loss. The exact cause of the reduction is however not well understood and explained in literature. In order to study the effect of slotting on reduction of magnet loss under field weakening, loss computations are performed by employing the proposed analytical technique with different values of the phase advance or field weakening angle 'γ' from 0^0 to 90^0 in steps of 30^0. $\gamma = 0^0$ corresponds to the phase current being in phase with the back-emf of the machine. Fig.19 shows the comparison of magnet loss with increase in field weakening angle for the 18-slot 8-pole surface mounted PM machine, with magnet pole arc angle 'β_m' of 175 ^{0} expressed in electrical degrees. It is observed that the difference in loss from $\gamma = 0^0$ to $\gamma = 90^0$ is 3.41W, which is close to the no load magnet loss of 3.2W.

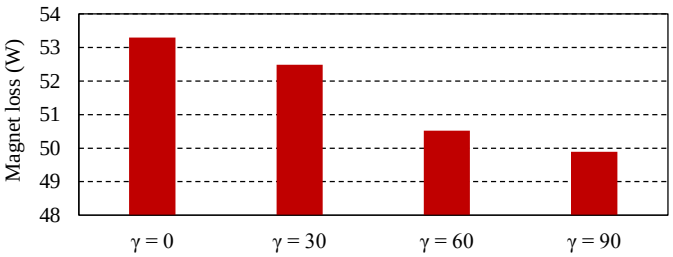

Fig. 19. Magnet losses comparison with increase in γ.

To apprehend the above observation, the magnet loss associated with the harmonics of the order which are integer multiples of the slot number 'N_s' is separated from the total loss. Fig.20 compares the difference in magnet loss due to the harmonics whose order are integer multiples of 'N_s' and the losses originated from all other harmonics with field weakening angle. It is clear from Fig.20 that the loss associated with harmonics which are integer multiples of 'N_s' is reducing with increase in field weakening angle, while the loss associated with other harmonics is more or less the same.

It can be shown that the harmonic contents of the source of the eddy current generation $\partial B_r/\partial t$ associated with the slotting effect [16] in the rotor reference are of the order $(\mu p \pm \upsilon N_s)\theta_r \pm \upsilon N_s \omega_r t$, where μ= 1, 3, 5… and υ= 1, 2, 3…Similarly from [8], the harmonic orders of $\partial B_r/\partial t$ due to armature reaction in the rotor reference are identified as $np_s\theta_r + (np_s - p)\omega_r t$, n = 2, 5, 8… for the forward rotating

harmonics and $np_s\theta_r + (np_s + p)\omega_r t$, n = 1, 4, 7... , for the backward rotating harmonics, respectively, where p_s is the number of pole pairs associated with the stator winding. For a given pole and slot number combination, and winding configuration, it can be shown that the slotting harmonics and a subset of the harmonics due to armature reaction have the same orders.

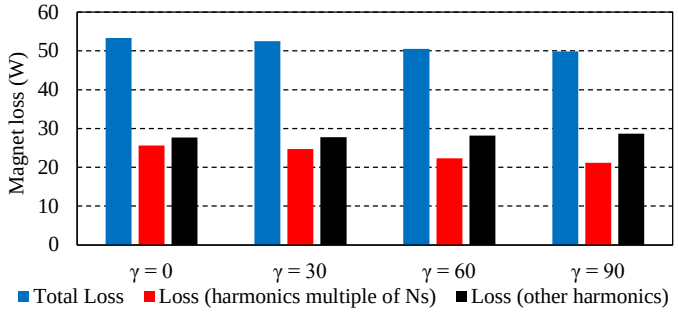

Fig.20. Separation of losses due to harmonics which are multiple of N_s.

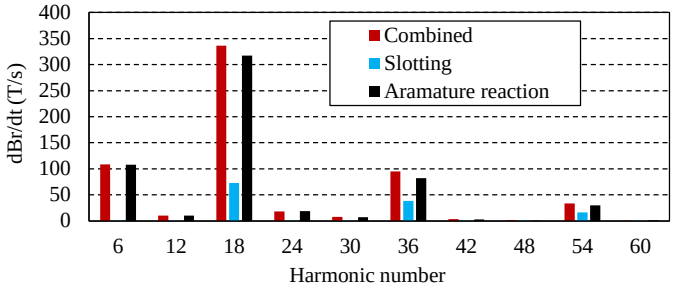

Fig.21. Comparison of harmonic distribution at $\gamma = 0^0$.

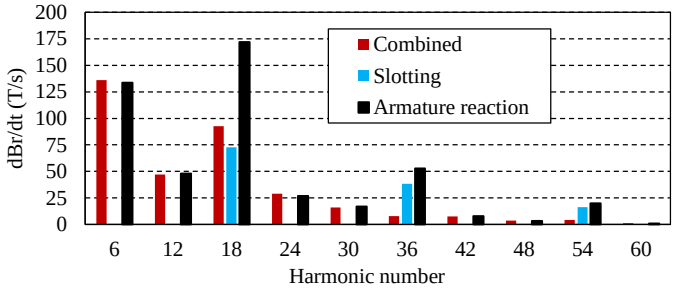

Fig.22. Comparison of harmonic distribution at $\gamma = +90^0$.

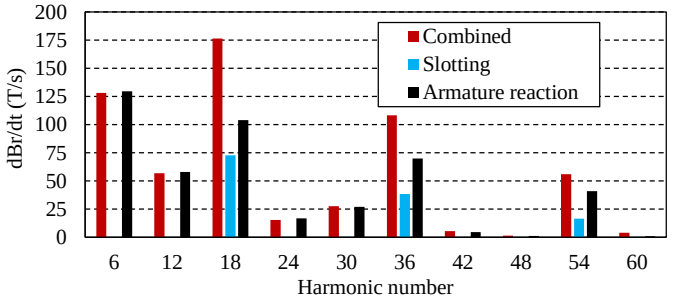

Fig.23. Comparison of harmonic distribution at $\gamma = -90^0$.

For the 18-slot 8-pole surface mounted PM machine considered in this study, p_s is equal to two, N_s = 18 and p = 4. Thus, the slotting harmonics are of the orders of 18, 36,54 …, and the armature reaction field seen by the rotor magnets also contains 18^{th}, 36^{th}, 54^{th},.., harmonics. Fig.21 compares the harmonic contents of $\partial B_r/\partial t$, evaluated from (14) at a point in the middle of the magnet '1', which results from the slotting harmonics and the harmonics due to armature reaction [8] when $\gamma = 0^0$. A similar comparison is shown in Fig.22 and Fig. 23 when $\gamma = +90^0$ and $\gamma = -90^0$ respectively. It is observed that the phase angle between the slotting harmonics and the armature reaction harmonics is close to 0^0 when $\gamma = -90^0$, which represents phase retarding. This angle reaches 90^0 when $\gamma = 0^0$, and becomes close to 180^0 when $\gamma = +90^0$. Since the magnitude of $\partial B_r/\partial t$ harmonics of the same order is a vector sum of the slotting component and the armature reaction component, the influence of slotting harmonics on the eddy current loss will depend on operation condition. In the field weakening operation when $\gamma > \sim 20^0$, the presence of the slotting harmonics tends to reduce the armature reaction harmonics of the same orders, and hence lead to the reduction of the eddy current loss in the rotor magnets.

VII. Conclusion

The 3D analytical method for predicting magnet eddy current loss has been developed and validated by 3D time-stepped transient FE analysis. The model is computationally efficient and hence suitable for evaluating the variation of eddy current loss in magnet with number of axial and circumferential segmentations. The accuracy of the results from the developed model justifies the negligence of tangential magnetic field inside the magnet and also the eddy current reaction effect at the operating conditions for the PM machine under study. The developed prediction technique has been validated by the experimental results. It has also been shown that the phase angles of the harmonics associated with slotting vary closely from 0^0 to 180^0 as the field weakening angle is increased from -90^0 to $+90^0$. Consequently, the presence of slotting harmonics reduces the eddy current loss under deep field weakening conditions.

References

[1] K. Atallah, J. Wang, and D. Howe, "Torque-ripple minimization in modular permanent-magnet brushless machines," IEEE Trans. Ind. Appl., vol. 39, pp. 1689-1695, 2003.

[2] R. Wrobel and P. H. Mellor, "Design Considerations of a Direct Drive Brushless Machine With Concentrated Windings," IEEE Trans. Energy Convers., vol. 23, pp. 1-8, 2008.

[3] K. Yoshida, Y. Hita, and K. Kesamaru, "Eddy-current loss analysis in PM of surface-mounted-PM SM for electric vehicles," IEEE Trans. Magn., vol. 36, pp. 1941-1944, 2000.

[4] Z. Nannan, Z. Q. Zhu, and L. Weiguo, "Rotor Eddy Current Loss Calculation and Thermal Analysis of Permanent Magnet Motor and Generator," IEEE Trans. Magn., vol. 47, pp. 4199-4202, 2011.

[5] H. Toda, X. Zhenping, J. Wang, K. Atallah, and D. Howe, "Rotor eddy-current loss in permanent magnet brushless machines," IEEE Trans. Magn., vol. 40, pp. 2104-2106, 2004.

[6] Z. Q. Zhu, K. Ng, N. Schofield, and D. Howe, "Improved analytical modelling of rotor eddy current loss in brushless machines equipped with surface-mounted permanent magnets," IEE Electr. Power Appl., vol. 151, pp. 641-650, 2004.

[7] D. Ishak, Z. Q. Zhu, and D. Howe, "Eddy-current loss in the rotor magnets of permanent-magnet brushless machines having a fractional number of slots per pole," IEEE Trans. Magn., vol. 41, pp. 2462-2469, 2005.

[8] J. Wang, K. Atallah, R. Chin, W. M. Arshad, and H. Lendenmann, "Rotor Eddy-Current Loss in Permanent-Magnet Brushless AC Machines," IEEE Trans. Magn., vol. 46, pp. 2701-2707, 2010.
[9] F. Dubas and A. Rahideh, "Two-Dimensional Analytical Permanent-Magnet Eddy-Current Loss Calculations in Slotless PMSM Equipped With Surface-Inset Magnets," IEEE Trans. Magn., vol. 50, pp. 54-73, 2014.
[10] Z. Q. Zhu, K. Ng, N. Schofield, and D. Howe, "Analytical prediction of rotor eddy current loss in brushless machines equipped with surface-mounted permanent magnets. I. Magnetostatic field model," in Proc. IEEE ICEM, 2001, pp. 806-809 vol.2.
[11] Z. X. Fang, Z. Q. Zhu, L. J. Wu, and Z. P. Xia, "Simple and accurate analytical estimation of slotting effect on magnet loss in fractional-slot surface-mounted PM machines," in Proc. IEEE ICEM, 2012, pp. 464-470.
[12] D. Zarko, D. Ban, and T. A. Lipo, "Analytical Solution for Cogging Torque in Surface Permanent-Magnet Motors Using Conformal Mapping," IEEE Trans. Magn., vol. 44, pp. 52-65, 2008.
[13] K. Boughrara, R. Ibtiouen, x, D. arko, O. Touhami, and A. Rezzoug, "Magnetic Field Analysis of External Rotor Permanent-Magnet Synchronous Motors Using Conformal Mapping," IEEE Trans. Magn., vol. 46, pp. 3684-3693, 2010.
[14] Z. Q. Zhu, L. J. Wu, and Z. P. Xia, "An Accurate Subdomain Model for Magnetic Field Computation in Slotted Surface-Mounted Permanent-Magnet Machines," IEEE Trans. Magn., vol. 46, pp. 1100-1115, 2010.
[15] L. J. Wu, Z. Q. Zhu, D. Staton, M. Popescu, and D. Hawkins, "An Improved Subdomain Model for Predicting Magnetic Field of Surface-Mounted Permanent Magnet Machines Accounting for Tooth-Tips," IEEE Trans. Magn., vol. 47, pp. 1693-1704, 2011.
[16] L. J. Wu, Z. Q. Zhu, D. Staton, M. Popescu, and D. Hawkins, "Analytical Modeling and Analysis of Open-Circuit Magnet Loss in Surface-Mounted Permanent-Magnet Machines," IEEE Trans. Magn., vol. 48, pp. 1234-1247, 2012.
[17] L. J. Wu, Z. Q. Zhu, D. Staton, M. Popescu, and D. Hawkins, "Analytical Model for Predicting Magnet Loss of Surface-Mounted Permanent Magnet Machines Accounting for Slotting Effect and Load," IEEE Trans. Magn., vol. 48, pp. 107-117, 2012.
[18] J. D. Ede, K. Atallah, G. W. Jewell, J. Wang, and D. Howe, "Effect of Axial Segmentation of Permanent Magnets on Rotor Loss in Modular Permanent-Magnet Brushless Machines," IEEE Trans. Ind. Appl., vol. 43, pp. 1207-1213, 2007.
[19] J. Wang, F. Papini, R. Chin, W. M. Arshad, and H. Lendenmann, "Computationally efficient approaches for evaluation of rotor eddy current loss in permanent magnet brushless machines," in Proc. IEEE ICEM, 2009, pp. 1-6.
[20] M. Mirzaei, A. Binder, and C. Deak, "3D analysis of circumferential and axial segmentation effect on magnet eddy current losses in permanent magnet synchronous machines with concentrated windings," in Proc. IEEE ICEM, 2010, pp. 1-6.
[21] H. Wan-Ying, A. Bettayeb, R. Kaczmarek, and J. C. Vannier, "Optimization of Magnet Segmentation for Reduction of Eddy-Current Losses in Permanent Magnet Synchronous Machine," IEEE Trans. Energy Convers., vol. 25, pp. 381-387, 2010.
[22] K. Yamazaki and Y. Fukushima, "Effect of Eddy-Current Loss Reduction by Magnet Segmentation in Synchronous Motors With Concentrated Windings," IEEE Trans. Ind. Appl., vol. 47, pp. 779-788, 2011.
[23] M. Mirzaei, A. Binder, B. Funieru, and M. Susic, "Analytical Calculations of Induced Eddy Currents Losses in the Magnets of Surface Mounted PM Machines With Consideration of Circumferential and Axial Segmentation Effects," IEEE Trans. Magn., vol. 48, pp. 4831-4841, 2012.
[24] T. Okitsu, D. Matsuhashi, G. Yanhui, and K. Muramatsu, "Coupled 2-D and 3-D Eddy Current Analyses for Evaluating Eddy Current Loss of a Permanent Magnet in Surface PM Motors," IEEE Trans. Magn., vol. 48, pp. 3100-3103, 2012.
[25] J. Pyrhonen, H. Jussila, Y. Alexandrova, P. Rafajdus, and J. Nerg, "Harmonic Loss Calculation in Rotor Surface Permanent Magnets- ;New Analytic Approach," IEEE Trans. Magn., vol. 48, pp. 2358-2366, 2012.
[26] B. Aslan, E. Semail, and J. Legranger, "General Analytical Model of Magnet Average Eddy-Current Volume Losses for Comparison of Multiphase PM Machines With Concentrated Winding," IEEE Trans. Energy Convers., vol. 29, pp. 72-83, 2014.
[27] Z. Peng, G. Y. Sizov, H. Jiangbiao, D. M. Ionel, and N. A. O. Demerdash, "Calculation of Magnet Losses in Concentrated-Winding Permanent-Magnet Synchronous Machines Using a Computationally Efficient Finite-Element Method," IEEE Trans. Ind. Appl., vol. 49, pp. 2524-2532, 2013.
[28] K. Yamazaki, M. Shina, Y. Kanou, M. Miwa, and J. Hagiwara, "Effect of Eddy Current Loss Reduction by Segmentation of Magnets in Synchronous Motors: Difference Between Interior and Surface Types," IEEE Trans. Magn., vol. 45, pp. 4756-4759, 2009.
[29] J. Wang, V. I. Patel, and W. Weiya, "Fractional-Slot Permanent Magnet Brushless Machines with Low Space Harmonic Contents," IEEE Trans. Magn., vol. 50, pp. 1-9, 2014.
[30] Y. Aoyama, K. Miyata, and K. Ohashi, "Simulations and experiments on eddy current in Nd-Fe-B magnet," IEEE Trans. Magn., vol. 41, pp. 3790-3792, 2005.
[31] P. Lazari, J. Wang, and C. Liang, "A Computationally Efficient Design Technique for Electric-Vehicle Traction Machines," IEEE Trans. Ind. Appl., vol. 50, pp. 3203-3213, 2014.

Sreeju S Nair (S'14) received B.Tech. degree in electrical and electronics engineering from National Institute of Technology, Calicut, in 2002, and received M.Tech. degree in electrical engineering from Indian Institute of Technology, Madras, India, in 2006, Currently he is working towards the Ph.D degree in the Dept. of Electronic and Electrical Engineering, The University of Sheffield, UK. His current research interests include eddy current loss evaluation and partial demagnetization of permanent-magnets in electrical machines.

Jiabin Wang (S'94–A'96–M'01–SM'03) received the B.Eng. and M.Eng. degrees from Jiangsu University of Science and Technology, Zhenjiang, China, in 1982 and 1986, respectively, and the Ph.D. degree from the University of East London, London, U.K., in 1996, all in electrical and electronic engineering. Currently, he is a Professor in Electrical Engineering at the University of Sheffield, U.K. His research interests range from motion control and electromechanical energy conversion to electric drives for applications in automotive, household appliances and aerospace sectors.

Robert Chin is currently the global research area manager at ABB corporate research, his main fields of interests are electromagnetics, thermal management, acoustics, dielectric and energy storage.

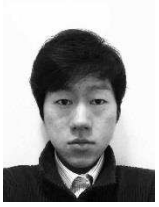

Liang Chen received the B.Eng. degree in 2006 and M.Eng degree in 2010, from Hefei University of Technology and Tsinghua University, China respectively. He is currently working towards the Ph.D. degree in the Department of Electronic and Electrical Engineering, The University of Sheffield, UK on design optimization of EV traction machines.

Tianfu Sun (S'15–M'16) received B.Eng. degree in mechanical engineering and M.Sc. degree in civil engineering from Dalian University of Technology, Dalian, China, in 2009 and 2012, respectively. He received Ph.D.in electrical engineering from The University of Sheffield, U.K. in 2016 and is now working as a post-doctoral research associate there. His current research interests include electric/hybrid vehicle drives, power-electronic control of electric machines, sensor less drives and artificial intelligence.